Astronomy & Astrophysics

Hint of 150 MHz radio emission
from the Neptune-mass extrasolar transiting planet HAT-P-11b[⋆]

A. Lecavelier des Etangs[1,2], S. K. Sirothia[3], Gopal-Krishna[3], and P. Zarka[4]

[1] CNRS, UMR 7095, Institut d'Astrophysique de Paris, 98bis boulevard Arago, 75014 Paris, France
e-mail: lecaveli@iap.fr
[2] UPMC Univ. Paris 6, UMR 7095, Institut d'Astrophysique de Paris, 98bis boulevard Arago, 75014 Paris, France
[3] National Centre for Radio Astrophysics, TIFR, Post Bag 3, Pune University Campus, Pune 411007, India
[4] LESIA, Observatoire de Paris, CNRS, UPMC, Université Paris Diderot, 5 place Jules Janssen, 92190 Meudon, France

ABSTRACT

Since the radio-frequency emission from planets is expected to be strongly influenced by their interaction with the magnetic field and corona of the host star, the physics of this process can be effectively constrained by making sensitive measurements of the planetary radio emission. Up to now, however, numerous searches for radio emission from extrasolar planets at radio wavelengths have only yielded negative results. Here we report deep radio observations of the nearby Neptune-mass extrasolar transiting planet HAT-P-11b at 150 MHz, using the Giant Meterwave Radio Telescope (GMRT). On July 16, 2009, we detected a 3σ emission whose light curve is consistent with an eclipse when the planet passed behind the star. This emission is at a position 14″ from the transiting exoplanet's coordinates; thus, with a synthetized beam of $FWHM \sim 16″$, the position uncertainty of this weak radio signal encompasses the location of HAT-P-11. We estimate a 5% false positive probability that the observed radio light curve mimics the planet's eclipse light curve. If the faint signature is indeed a radio eclipse event associated with the planet, then its flux would be 3.87 mJy ± 1.29 mJy at 150 MHz. However, our equally sensitive repeat observations of the system on November 17, 2010 did not detect a significant signal in the radio light curve near the same position. This lack of confirmation leaves us with the possibility of either a variable planetary emission, or a chance occurrence of a false positive signal in our first observation. Deeper observations are required to confirm this hint of 150 MHz radio emission from HAT-P-11b.

Key words. planetary systems – stars: coronae – techniques: interferometric

1. Introduction

The importance of the physics behind star-planet interaction, in conjunction with theoretical predictions available for radio emission from a large number of extrasolar planets (Grießmeier et al. 2007), has provided the impetus for making searches for decameter- and meter-wavelength radio emission from a few carefully selected extrasolar planets (Bastian et al. 2000; Ryabov et al. 2004; Winterhalter et al. 2005; George & Stevens 2007; Lazio & Farrell 2007; Smith et al. 2009; Lecavelier des Etangs et al. 2009, 2011; Lazio et al. 2010a,b). Using the scaling laws (Zarka et al. 2001; Zarka 2007), radio emission from extrasolar planets orbiting close to their host stars could reach 10^3 to 10^5 times the radio output from Jupiter and hence be detectable with the most sensitive existing radio telescopes. Even at large orbital distances ($\gtrsim 1$ AU), radio emissions from rapidly rotating planets orbiting stars with high X-UV brightness could be detectable (Nichols 2011). Nonetheless, in the absence of detection, the theoretical estimates made for exoplanetary radio cyclotron emission are based on a host of unknowns, such as the stellar wind, coronal density, and stellar and planetary magnetic fields.

Up to now, various programs to search for radio emission have given negative results. The telescopes used include the UTR-2 (10 MHz, $\sigma \sim 1.6$ Jy), the VLA (74 MHz, $\sigma \sim 50$ mJy;

325 MHz, $\sigma \sim 0.6$ mJy; 1425 MHz, $\sigma \sim 15\,\mu$Jy), and the Giant Meterwave Radio Telescope (GMRT; see review in Lazio et al. 2009; and Zarka 2011). Interferometric observations of high sensitivity and high resolution using the GMRT, which is a 30-km baseline Y-shaped array consisting of 30 steerable dishes of 45-m diameter each providing an effective area around 30 000 m² (Swarup 1990), seem very promising for this purpose.

The planet HAT-P-11b is 4.3 Earth radii planet (Deming et al. 2011) orbiting a bright and metal-rich K4 dwarf with a 4.89 day period on an eccentric orbit ($e \approx 0.2$). This transiting planet located 38 pc away from us was discovered by Bakos et al. (2010) with ground-based photometry using the HATNet survey (Bakos et al. 2004) and was confirmed by Dittmann et al. (2009). With a mass of about 26 Earth mass, this planet belongs to the so-called "hot-Neptune" category. The host star HAT-P-11 is metal rich ([Fe/H] = +0.31 ± 0.05). Its *Kepler* photometry has shown that the stellar surface has active spotted areas at fixed latitudes (Deming et al. 2011; Sanchis-Ojeda & Winn 2011).

The planet's orbital axis is highly misaligned from the star's rotation axis, with a sky projected obliquity of $\lambda \sim 103°$ (Winn et al. 2010; Hirano et al. 2011). Nonetheless, the orbital plane is seen almost edge-on from the Earth and thus HAT-P-11 b is eclipsed by the star for about two hours during each orbital cycle. The planet's eclipses can be used to discriminate any planetary emission from the stellar emission; the same technique has been used extensively for measuring planetary infrared emission using various space and ground-based telescopes (Deming et al. 2005; Charbonneau et al. 2005; Sing et al. 2008).

---

2. Radio observations at 150 MHz and data analysis

We observed the HAT-P-11 field with the GMRT before, during, and after the planetary eclipse, from July 16, 2009, 15h30m UT to July 17, 1h00m UT. The data consist of about 10^9 visibility measurements along the 435 baselines of the GMRT aperture-synthesis array. The integration time was 2 s and the central frequency was set at 150 MHz with a bandwidth of 16 MHz. The short integration time allows us to construct a radio light curve (see below), which is also sensitive to any large radio flares.

Because the July 2009 run provided a $\sim3\sigma$ detection near the HAT-P-11 position and a radio light curve consistent with an eclipse of the planet HAT-P-11b (Sect. 3), we decided to carry out a second observation of the same field. This second run was scheduled on November 17, 2010, from 6h00m to 16h00m UT. Combining the two observation runs, the total data acquisition time on the target field is about 20 h, including the total acquisition for the durations of the two eclipses (about 4 h).

The data reduction was done mainly using the `AIPS++` package. We used 3C48 as the primary flux density and bandpass calibrator, taking a flux density of 64.42 Jy at 148 MHz. The phase calibrator was the source 2038+513 which was observed repeatedly during the runs.

While calibrating the data, bad data points were flagged at various stages. The data for antennas with relatively large errors in antenna-based gain solutions were examined and flagged over certain time ranges. Some baselines were flagged based on closure errors on the bandpass calibrator. Channel and time-based flagging of the data points corrupted by radio frequency interference (RFI) was done by applying a median filter with a 6σ threshold. Residual errors above 5σ were also flagged after a few rounds of imaging and self-calibration. The final image was made after several rounds of phase self-calibration and one round of amplitude self-calibration where the data were normalized by the median gain found for the entire data. The final image was also corrected for the primary beam shape taken to be a Gaussian with FWHM of 173.83′ at 150 MHz.

After the final imaging stage, we generated light curves of several emission peaks detected around the HAT-P-11 position: one light curve of the peak source detected in July 2009 within a synthesized beam from HAT-P-11 (at such a low signal to noise ratio, the accuracy on the position of a detected source is approximately the beam size), and the light curves of 14 emission peaks with similar S/N and detected around HAT-P-11 in both observations. These last light curves can be used for comparison purposes and validation of the statistics. To obtain these light curves, we calculated model visibilities using the sources detected in the entire field-of-view excluding a synthesized beam-wide region centered on the desired locations (α_0, δ_0); we then subtracted this model from the final calibrated visibility data. The residual visibility data (RVD) were then phase-centered on α_0, δ_0 and averaged for desired time bins to generate the light curves.

3. Results

3.1. Observations of July 16, 2009

Figure 1 shows the 150 MHz map of the field around HAT-P-11 obtained from the observations on July 16, 2009. A faint source is detected at the coordinates α = 19h50m51.0s, δ = +48°05′03″ (J2000), which are 14″ (about a beam width) northeast from the HAT-P-11 coordinates (α = 19h50m50.247s, δ = +48°04′51.08″). Figure 2 shows the 150 MHz light curve derived at the source position.
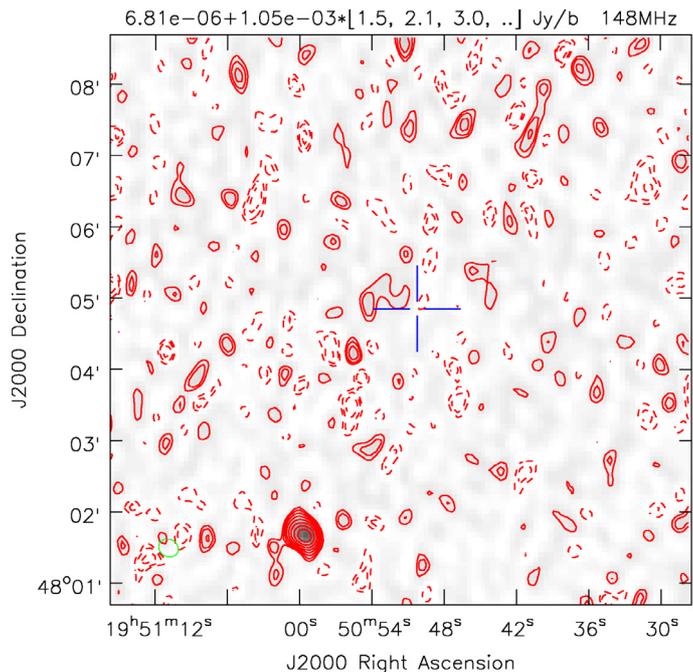
Fig. 1. GMRT image of the HAT-P-11 field at 150 MHz on July 16, 2009. The green ellipse in the lower-left corner shows the half-power beam width. The contour levels given at the top of the image are in units of Jy beam^{-1} and are defined as mean + rms × (n), where values of n are given in the brackets. Thus, the first, second, and third contours correspond to 1.5×1.05 mJy, 2.1×1.05 mJy, 3.0×1.05 mJy, etc. Negative contours appear as dashed lines.
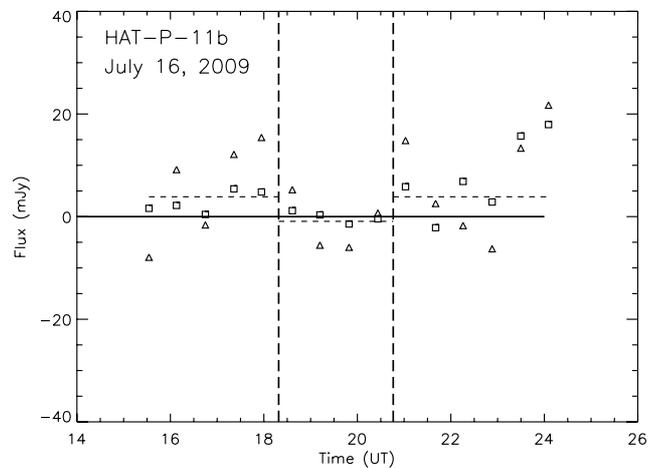

Fig. 2. Time series of the 150 MHz flux density measured on July 16, 2009, in the direction of the radio source near HAT-P-11. The measurements have been rebinned to 36 min. Triangles and squares correspond to the RR and LL polarizations, respectively. The two vertical long-dashed lines indicate the beginning and the end of the planet's eclipse behind the host star. The dashed horizontal lines show the box-shaped eclipse light curve fitted to the data points.

Over the full integration time, including the two-hour eclipse, the source has a mean flux of 2.45 ± 1.09 mJy (2.2σ detection). If we consider only the time outside the eclipse (Fig. 2), a mean flux of 3.87 ± 1.29 mJy (3σ) is measured. During the eclipse of the planet behind the host star, no emission was detected and the mean flux was found to be -0.92 ± 1.94 mJy, consistent with zero emission for this time interval. The light curve is thus in agreement with the expected light curve for a planetary
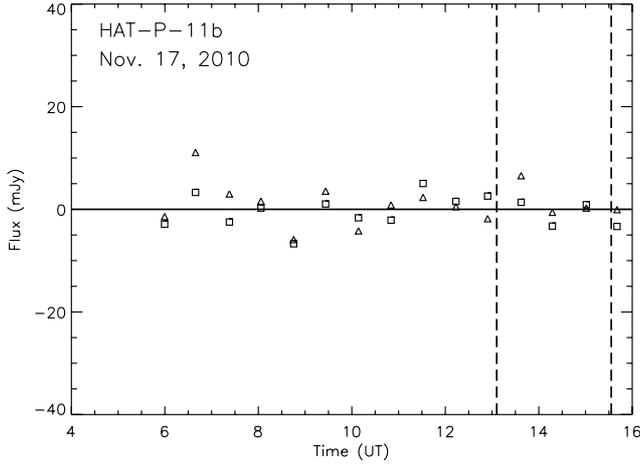
Fig. 3. Same as in Fig. 2, in the direction of HAT-P-11 on November 17, 2010. The mean of the flux density measurements is found to be 0.00 ± 1.19 mJy. Thus, no emission is detected towards or near HAT-P-11 in these observations.

Fig. 4. Time series of the 150 MHz flux density measured in the direction of one comparison source at $\alpha = 19h50m32.2s$, $\delta = +48°04'22''$ (J2000), at 183'' from HAT-P-11. The dashed horizontal lines show the mean values of flux density at the two observation epochs.

radio emission, eclipsed when the planet is known to be behind its host star. Thus, a straightforward, albeit heuristic, interpretation of the light curve would be a 3σ detection of the planet HAT-P-11 b at 150 MHz.

The position of the source exhibiting the eclipse light curve has been measured to be 14'' away from HAT-P-11. However, for such a faint source the positional accuracy is similar to the beam size of 16''. More precisely, from our experience with GMRT maps at 150 MHz, we derived an empirical expression for the positional accuracy on GMRT maps; at 90% confidence we found an accuracy on the position given by $Beamsize \times (1/SNR + 1/10)$, which is in agreement with the same relationship found on the VLA First Survey Catalog which reports[1] a 90% confidence positional accuracy of $Beamsize \times (1/SNR + 1/20)$. Applying this relationship to our measurement of the emission peak at 2.2σ and taking into account the 4'' pixel size, we find that the above measurement of the radio position can be consistent with the HAT-P-11 coordinates.

To assess the reliability of this detection, we also estimated the false-positive detection probability, i.e., the probability of observing a light curve of this shape for a constant radio emission with no real eclipse, but only an eclipse mimicked by the random noise along the radio light curve. This is calculated by estimating the probability that the mean flux during the eclipse is lower than zero, as observed. For this calculation we used the present estimate of the source flux, and the error bars for the times outside and during the eclipse. For the case of no real flux variation, our analysis shows that the probability of the mean flux during the eclipse being below zero is only 4.8%. We conclude a 5% false positive probability of eclipse detection in the observed 150 MHz light curve at the position coincident (within the errors) with the planet HAT-P-11b.

We also computed the χ^2 of two different models fitting the light curve data with a 339-s sampling time providing a total of 190 measurements. In the first single-parameter model, we assume a constant flux level for the entire light curve, corresponding to the hypothesis that the radio source is not the planet and therefore the flux density is constant in time. We find a χ^2 of 186.6 for 189 degrees of freedom. In the second model, we
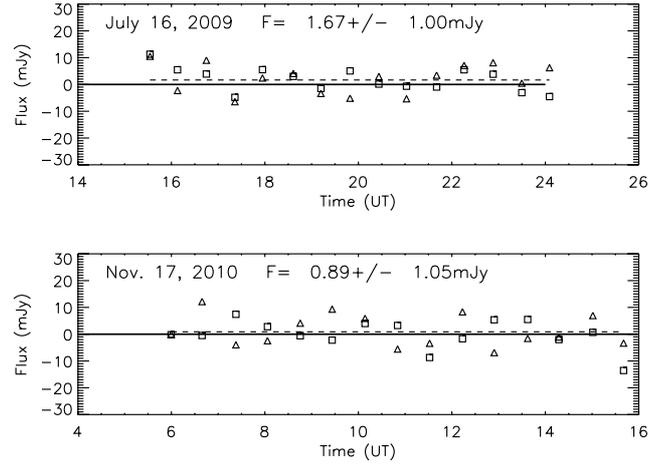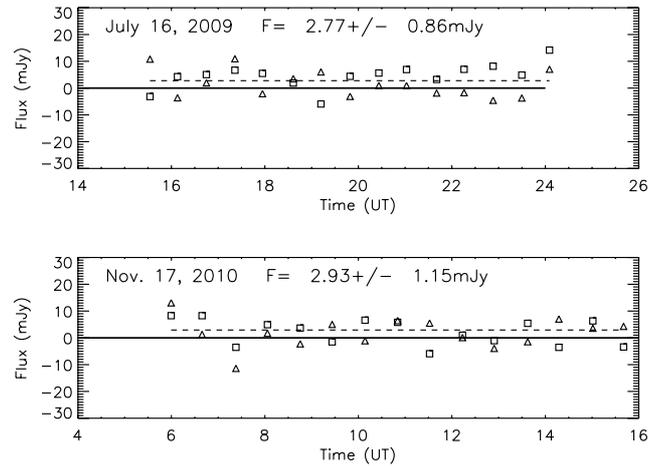
[1] http://sundog.stsci.edu/first/catalogs/readme.html

Fig. 5. Same as Fig. 4, but for the observed peak at $\alpha = 19h50m45.8s$, $\delta = +48°04'10''$ (J2000), at 61'' from HAT-P-11.

assume that the source is a planetary emission and the flux density during the eclipse is fitted by a second parameter, larger than or equal to zero. With this two-parameter model we find a χ^2 of 182.8 for 188 degrees of freedom. Using the F-test, we conclude that the decrease of χ^2 by 3.8 favors the second model with a 95.0% confidence level, which is consistent with the conclusion based on the false positive probability calculated above.

To make the above analysis more rigorous, we also derived the radio light curve for 14 sources seen within a few arc minutes around HAT-P-11 and detected at both observation epochs. The measured fluxes of these comparison sources are in the range ~1 to 3 mJy. Four examples of light curves are given in Figs. 4 to 7. We found that the false positive probabilities computed for these directions are uniformly distributed between 0 and 1, validating our approach. Thus, to a 95% confidence limit, the detected signal is consistent with a 150 MHz radio emission associated with the extrasolar planet HAT-P-11b.

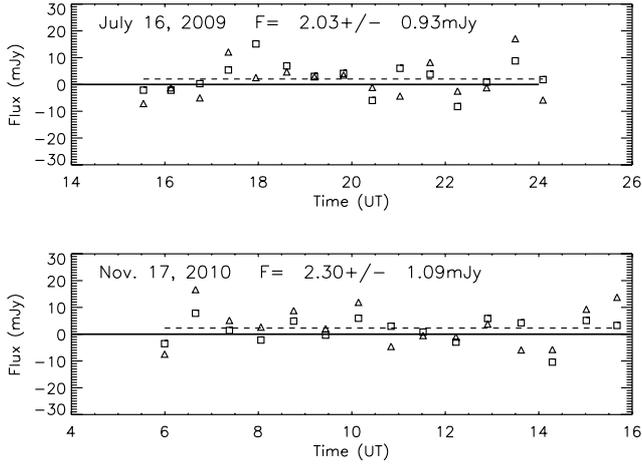**Fig. 6.** Same as Fig. 4, but for α = 19h50m56.9s, δ = +48°05′46″ (J2000), at 87″ from HAT-P-11.
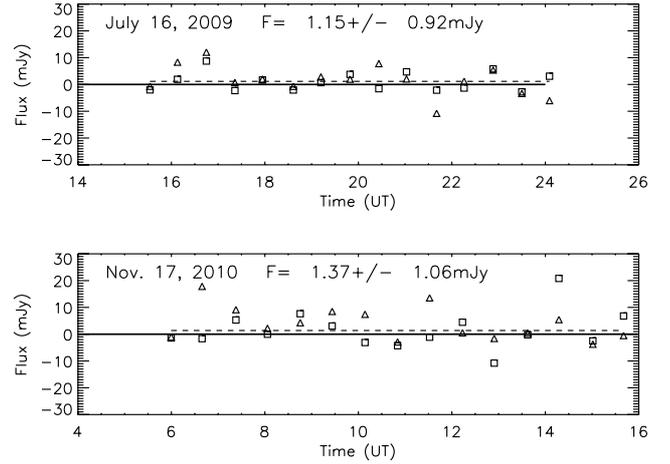
Fig. 7. Same as Fig. 4, but for α = 19h50m58.9s, δ = +48°02′26″ (J2000), at 169″ from HAT-P-11.

3.2. Observations of November 17, 2010

In the full-synthesis GMRT observations of November 17, 2010, we did not detect any emission toward HAT-P-11 or nearby directions within a synthesized beam. On this occasion, the nearest detected radio source lies at 27.5″ from HAT-P-11, and has a flux of 1.78 ± 1.01 mJy. The light curve of this source at 150 MHz does not show any eclipse-like signature. Therefore, we are led to conclude that in these observations of HAT-P-11 we did not detect the radio source and its associated eclipse event we had seen on July 16, 2009.

3.3. False positive or variability?

There are two plausible explanations for the discrepancy between the results of the two epochs. First, a false positive detection at the first epoch cannot be completely ruled out given the estimated false positive probability of 5% (Sect. 3.1). Moreover, the source is close to the detection limit. So a false detection due to noise cannot be excluded at present.

The second interpretation invokes the general variability of planetary radio emission at low frequencies. The variable nature of the radio emission is indeed predicted by models including the observed variability of the stellar magnetic field. For instance, in the case of HD 189733b Fares et al. (2010) showed that the observed variations in the position of the so-called "source surface" (the stellar surface beyond which the magnetic field becomes purely radial) produce variations in the expected radio flux. Thus, in the case of HAT-P-11, if the discrepancy between the results of July 2009 and November 2010 is due to variability of the radio emission, we may have actually detected sporadic emission from the extrasolar planet at 150 MHz on July 16, 2009. However, the variable nature of the emission precludes a claim of detection; we are left with a hint, and we must wait for further, possibly even more sensitive observations.

4. Ephemeris uncertainties

The characteristics and ephemeris of the planet's orbit are needed to compute the eclipse light curve. Here we used the orbit's eccentricity e and the longitude of periastron ω provided in the discovery paper by Bakos et al. (2010): $e \cos \omega = 0.201 \pm 0.049$ and $e \sin \omega = 0.051 \pm 0.092$. The more recent

observations of transits of HAT-P-11 b using the *Kepler* satellite provide new ephemeris for the transit central time T_0 and orbital period P (Deming et al. 2011; Sanchis-Ojeda & Winn 2011). We used the following values given in Deming et al. (2011): $T_0 = 2\,454\,605.89155$ (BJD) and $P = 4.8878018$ days. The difference between the eclipse time calculated using these new values and the time calculated using the T_0 and P given in Bakos et al. is not more than 1.5 min.

More importantly, the new measurements using the *Kepler* photometric data yield a smaller impact parameter $b_1 = a \cos i / R_p$, where a is the semi-major axis, i the orbit's inclination, and R_p the planet's radius. A smaller impact parameter leads to a longer eclipse duration. Using the new values, we found an eclipse duration of 2 h and 27 min, which is 38 min longer than the previous estimates using the Bakos et al. (2010) impact parameter.

By far, the largest uncertainty in computing the eclipse time arises from the uncertainty in the orbital eccentricity and longitude of the periastron, the uncertainty reaching up to $\pm$3h30m in the extreme cases. Unfortunately, the eclipse amplitude in the infrared may be too faint to be detected using the *Spitzer* Space Telescope (Deming et al. 2011). Only new radial velocity measurements in the coming years may improve the accuracy of the orbital eccentricity. Here, we used the best published values given by Bakos et al. (2010) and used the eclipse phase $\phi = 0.628$, where $\phi = 0$ corresponds to the central transit of the planet in front of the host star.

5. Discussion

5.1. Radio emission frequency

The principal mechanism put forward for planetary radio emission is electron-cyclotron maser radiation. It occurs at the local gyrofrequency $f_g = 2.8 \left(B_p / 1\,\text{G} \right)$ MHz, where B_p is the planet's magnetic field. The detection at a frequency of 150 MHz would then correspond to a planetary magnetic field of around 50 G.

We recall that the Jovian magnetic field estimated from the radio frequency cut-off in its cyclotron emission is around 14 G. Thus, the present tentative radio detection requires a magnetic field for HAT-P-11 b ($\sim$50 G) that is of the same order of magnitude, albeit slightly stronger than that of Jupiter. We have no clues to the possible origin of a magnetic field of this strength,

although we can emphasize here the particularities of this planet which has a significantly higher density than Jupiter, and orbits a metal-rich star ([Fe/H] = +0.31 ± 0.05). The planet HAT-P-11 b is consequently expected to have a high abundance of heavy elements and a large core mass (Guillot et al. 2006). Taken all together, its peculiarities (eccentric and highly inclined orbit, metal-rich host star, short orbital period, etc.) make this planet different enough from any planet in our own solar system that it is difficult to make a reasonable guess of its magnetic field strength. Hence the requirement of a magnetic field 3 to 4 times Jupiter's seems quite plausible.

5.2. Emission flux

Several mechanisms for exoplanet radio emissions have been considered by Grießmeier et al. (2007): stellar wind (SW)-magnetosphere magnetic interaction, SW-magnetosphere kinetic interaction, and coronal mass ejection (CME)-magnetosphere kinetic interaction. Application to HAT-P-11 b of the scaling law extrapolations of Grießmeier et al. (2007) lead to predicted radio flux densities of 14 mJy for the SW-magnetosphere magnetic interaction, 1 mJy for the CME-magnetosphere kinetic interaction, and ≪1 mJy for the SW-magnetosphere kinetic interaction (note that these are mere orders of magnitude). The first two values are of the same order of magnitude as the ~4 mJy flux density tentatively detected here.

Alternatively, if the stellar magnetic field is strong enough, the planet may induce electron precipitations and thus radio emission in the star's magnetic field (Zarka et al. 2001; Zarka 2007). This may be the case for HAT-P-11 b whose semi-major axis is only 0.053 au. The stellar magnetosphere could even extend beyond the planet's orbit. In the framework of the Jardine & Cameron (2008) model in which the radio emission is caused by interaction of the planetary magnetosphere with the stellar corona in which it is embedded, we can derive typical values for the resulting radio signal from HAT-P-11 b. Because HAT-P-11 is a slowly rotating star (Bakos et al. 2010) with a rotation period of $30.5^{+4.1}_{3.2}$ days (Sanchis-Ojed & Winn 2011), the planet's velocity relative to the star's magnetosphere is $v_p - v_* = 99 \, \mathrm{km \, s^{-1}}$ (i.e., three times higher than that of HD 189733b). Taking a 10% efficiency for conversion of the power of the accelerated electrons into radio emission within an emission beam solid angle of 1.6 steradian, a stellar magnetic field $B_* = 40$ G as measured for the K-type star HD 189733 (Moutou et al. 2007), and a stellar density at the base of the corona equal to the solar value, we obtain a predicted radio flux in this model of the order of 13 mJy from HAT-P-11 b, again similar to the tentative detection reported here.

We conclude that a radio emission of the hot-Neptune HAT-P-11 b at a level of a few milli-Jansky level is consistent with existing theoretical predictions, in particular the predictions based on the cyclotron maser instability (CMI) of energetic electrons accelerated through the interaction of the planetary magnetic field with the stellar magnetic field, or CMEs.

6. Conclusion

Although we are not able to draw a definitive conclusion on 150 MHz radio emission from HAT-P-11 b, at the very least the hint of radio detection presented here identifies HAT-P-11 b as a prime candidate for many follow-up observations in the near future. The priority is to try to confirm the present tentative detection, via re-observation with GMRT at 150 MHz

and/or new observations with LOFAR in the 30–250 MHz range (providing a 1–100 mJy sensitivity depending on the observation parameters used; van Haarlem et al. 2012) and UTR-2 in the 10–30 MHz range (providing a sensitivity of ~100 mJy; Ryabov et al. 2004). The observed spectral range can also be extended toward shorter wavelengths using GMRT, with even higher sensitivities of ~1 mJy at 240 MHz and ~50 μJy at 614 MHz (e.g., Lecavelier des Etangs et al. 2009). Observations over a broad range of frequencies will, with any luck, allow confirmation of the existence of the emission and better constraints on the planetary magnetic field strength and determination of the radio spectral index.

The future observations should also be distributed at multiple epochs and at different orbital phases of the planet to characterize the suspected variability of the radio emission in terms of duty cycle, as well as the radio emission as a function of the star-planet angle and the emission directivity (CMI produces narrowly beamed radio emission). In this context, Hess & Zarka (2011) have analyzed all the observables that could be derived from a broadband dynamic spectrum with a sufficient signal-to-noise ratio.

In the long term, it should be possible to investigate if the radio emission from extrasolar planetary systems correlates with the stellar spot activity. In this context, HAT-P-11 represents the target of choice because the *Kepler* mission has recently demonstrated the possibility of following the spot activity and perhaps even of drawing the butterfly diagram of surface spots for this star (Deming et al. 2011; Sanchis-Ojeda & Winn 2011).

Radio observations of different types of exoplanets are also crucial for comparative exoplanetology. For instance, observations of the other transiting hot-Neptune GJ436 b (Gillon et al. 2007) will allow comparison with a planet similar in mass but orbiting an M-dwarf star which is half the mass and radius of HAT-P-11 and known to have a strong Far-UV and Lyman-α output (Ehrenreich et al. 2010). With a 6.55 Earth mass, the nearby exoplanet GJ1214 b should also provide an opportunity to undertake search for radio emission from a water-rich lower mass super-Earth planet (Charbonneau et al. 2009; Désert et al. 2011). In the near future, more sensitive observations at even lower frequencies will become feasible with the LOFAR observatory, providing a great boost to exoplanetary research.

References

Bakos, G., Noyes, R. W., Kovács, G., et al. 2004, PASP, 116, 266
Bakos, G. Á., Torres, G., Pál, A., et al. 2010, ApJ, 710, 1724
Bastian, T. S., Dulk, G. A., & Leblanc, Y. 2000, ApJ, 545, 1058
Charbonneau, D., Allen, L. E., Megeath, S. T., et al. 2005, ApJ, 626, 523
Charbonneau, D., Berta, Z. K., Irwin, J., et al. 2009, Nature, 462, 891
Deming, D., Seager, S., Richardson, L. J., & Harrington, J. 2005, Nature, 434, 740
Deming, D., Sada, P. V., Jackson, B., et al. 2011, ApJ, 740, 33
Désert, J.-M., Bean, J., Miller-Ricci Kempton, E., et al. 2011, ApJ, 731, L40
Dittmann, J. A., Close, L. M., Green, E. M., Scuderi, L. J., & Males, J. R. 2009, ApJ, 699, L48

Ehrenreich, D., Lecavelier des Etangs, A., & Delfosse, X. 2011, A&A, 529, A80
Fares, R., Donati, J.-F., & Moutou, C. 2010, MNRAS, 406, 409
George, S. J., & Stevens, I. R. 2007, MNRAS, 382, 455
Gillon, M., Pont, F., Demory, B.-O., et al. 2007, A&A, 472, L13
Grießmeier, J.-M., Zarka, P., & Spreeuw, H. 2007, A&A, 475, 359
Guillot, T., Santos, N. C., Pont, F., et al. 2006, A&A, 453, L21
Hess, S. L. G., & Zarka, P. 2011, A&A, 531, A29
Hirano, T., Narita, N., Shporer, A., et al. 2011, PASJ, 63, 531
Jardine, M., & Cameron, A. C. 2008, A&A, 490, 843
Lazio, T. J. W., & Farrell, W. M. 2007, ApJ, 668, 1182
Lazio, J., Bastian, T., Bryden, G., et al. 2009, astro2010: The Astronomy and Astrophysics Decadal Survey, 2010, 177
Lazio, T. J. W., Carmichael, S., Clark, J., et al. 2010a, AJ, 139, 96
Lazio, T. J. W., Shankland, P. D., Farrell, W. M., & Blank, D. L. 2010b, AJ, 140, 1929
Lecavelier des Etangs, A., Sirothia, S. K., Gopal-Krishna, & Zarka, P. 2009, A&A, 500, L51

Lecavelier des Etangs, A., Sirothia, S. K., Gopal-Krishna, & Zarka, P. 2011, A&A, 533, A50
Moutou, C., Donati, J.-F., Savalle, R., et al. 2007, A&A, 473, 651
Nichols, J. D. 2011, MNRAS, 414, 2125
Ryabov, V. B., Zarka, P., & Ryabov, B. P. 2004, Planet. Space Sci., 52, 1479
Sanchis-Ojeda, R., & Winn, J. N. 2011, ApJ, 743, 61
Sing, D. K., & López-Morales, M. 2009, A&A, 493, L31
Smith, A. M. S., Cameron, A. C., Greaves, J., et al. 2009, MNRAS, 395, 335
Swarup, G. 1990, Ind. J. Radio Space Phys., 19, 493
van Haarlem, M. P., Wise, M. W., Gunst, A., et al. 2012, A&A, submitted
Winn, J. N., Johnson, J. A., Howard, A. W., et al. 2010, ApJ, 723, L223
Winterhalter, D., Majid, W., Kuiper, T., et al. 2005, BAAS, 37, 1292
Zarka, P. 2007, Planet. Space Sci., 55, 598
Zarka, P. 2011, in Planetary Radio Emissions VII, eds. H. O. Rucker et al. (Vienna: Austrian Acad. Sci. Press), 287
Zarka, P., Treumann, R. A., Ryabov, B. P., & Ryabov, V. B. 2001, Ap&SS, 277, 293